LETTER

doi:10.1038/nature10583

Grid cells without theta oscillations in the entorhinal cortex of bats

Michael M. Yartsev[1], Menno P. Witter[2] & Nachum Ulanovsky[1]

Grid cells provide a neural representation of space, by discharging when an animal traverses through the vertices of a periodic hexagonal grid spanning the environment[1]. Although grid cells have been characterized in detail in rats[1–6], the fundamental question of what neural dynamics give rise to the grid structure remains unresolved. Two competing classes of models were proposed: network models, based on attractor dynamics[7–9], and oscillatory interference models, which propose that interference between somatic and dendritic theta-band oscillations (4–10 Hz) in single neurons transforms a temporal oscillation into a spatially periodic grid[10–13]. So far, these models could not be dissociated experimentally, because rodent grid cells always co-exist with continuous theta oscillations[4–6,14]. Here we used a novel animal model, the Egyptian fruit bat[15,16], to refute the proposed causal link between grids and theta oscillations. On the basis of our previous finding from bat hippocampus, of spatially tuned place cells in the absence of continuous theta oscillations[17], we hypothesized that grid cells in bat medial entorhinal cortex might also exist without theta oscillations. Indeed, we found grid cells in bat medial entorhinal cortex that shared remarkable similarities to rodent grid cells. Notably, the grids existed in the absence of continuous theta-band oscillations, and with almost no theta modulation of grid-cell spiking—both of which are essential prerequisites of the oscillatory interference models. Our results provide a direct demonstration of grid cells in a non-rodent species. Furthermore, they strongly argue against a major class of computational models of grid cells.

To elucidate the cellular and network mechanisms of grid cells in mammalian entorhinal cortex, we conducted electrophysiological recordings in a megabat, *Rousettus aegyptiacus* (Egyptian fruit bat). This bat species[15] belongs to a different suborder of bats than the big brown bat[16], the hippocampus of which we studied previously[17,18]. Therefore, to set the foundations for subsequent entorhinal recordings in this bat species, we first examined neural activity in hippocampal area CA1 (Fig. 1a). Bats crawled in a large arena (Fig. 1b) in search of food, and the activity of individual neurons was recorded using tetrodes (Supplementary Figs 1 and 2). Of all the well-isolated excitatory neurons in CA1, 36% were classified as place cells, becoming active when the bat entered a particular region of the environment (23 out of 64 cells with spatial information >0.5 bits per spike). Locations of individual place fields spanned the entire experimental arena (Fig. 1c), similar to place cells in rats[19]. High-frequency ripple oscillations (120–160 Hz) were present in the local field potential (LFP) during sleep (Supplementary Fig. 3a), and were very similar in their properties to ripples in rat hippocampus[20] (Supplementary Fig. 3 and Supplementary Text). Hippocampal theta oscillations in the LFP occurred in short, intermittent bouts (Fig. 1d), lasting typically ~1 s, and these bouts in the behaving bat were separated with an average 19-s interval (Supplementary Fig. 4a–d)—markedly different from the continuous theta oscillations observed in locomoting rats[21], but similar to the intermittent theta bouts in monkeys[22] and humans[23]. Because of the sparse occurrence of these bouts, theta oscillations were not evident in spectral analysis of the LFP, neither during sleep (Fig. 1e, left), during behavioural sessions (right), nor as a function of the bat's velocity (Fig. 1f). Thus, in agreement with our previous findings in big brown bats[17], we found that in Egyptian fruit bats, hippocampal place cells existed in the absence of continuous theta oscillations in the LFP.

We next turned to studying the medial entorhinal cortex (MEC) of bats, the region where grid cells are most prevalent in rats[1–6]. As a first step, we determined the anatomical location and borders of MEC (Fig. 2a and Supplementary Figs 5 and 6). Immunohistochemical staining revealed that: (1) similar to rats[24], the dorsal border of bat MEC (postrhinal border) was clearly identifiable by an abrupt change in layer structure (Supplementary Fig. 6b, d) and an abrupt transition in parvalbumin and calretinin staining (Fig. 2a and Supplementary Figs 5 and 6); and (2) similar to rats, the bat MEC had a densely packed layer II, sparser layers III and V, and a layer IV (*lamina dissecans*) with very few cell bodies (Supplementary Figs 5 and 6). Thus, the overall structure of bat MEC was very similar to that of rat MEC.

We targeted our tetrode recordings to the dorsal-most part of MEC: the region where we expected to find grid cells with the tightest and most pronounced grid structure, as in rats[1,2]. The positions of all

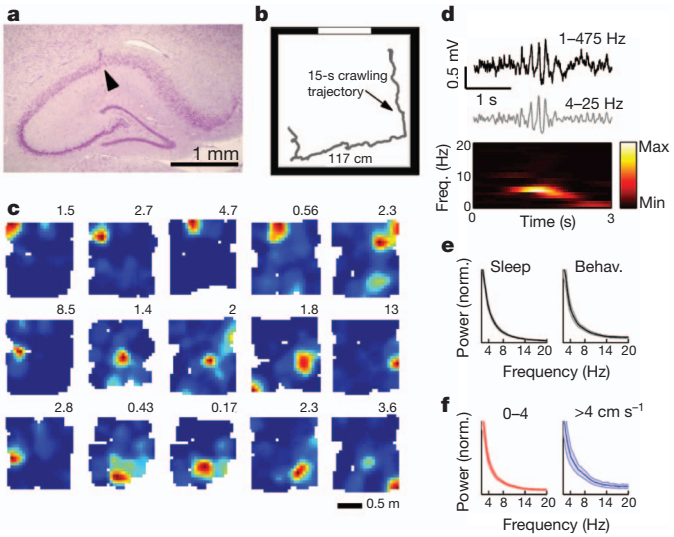

Figure 1 | Bat CA1 recordings demonstrate place cells but no continuous theta oscillations. **a**, Coronal section showing tetrode track in dorsal hippocampal area CA1 (arrowhead). **b**, Behavioural arena (117 × 117 cm) with white cue card. Grey line shows example 15-s crawling trajectory. **c**, Firing rate maps of 15 place cells, colour-coded from zero (blue) to maximum firing rate (red; value indicated). **d**, Example theta bout recorded during locomotion. Top: wideband LFP trace (1–475 Hz, black); middle, filtered trace (4–25 Hz, grey); bottom, spectrogram (frequency × time). **e**, LFP power spectrum during sleep (left) and behaviour (right) for all recording sites (mean ± s.e.m.). **f**, LFP power spectrum separated according to bat's velocity (indicated); normalized to power at 2 Hz. Note absence of peak at theta frequency.

[1]Department of Neurobiology, Weizmann Institute of Science, Rehovot 76100, Israel. [2]Kavli Institute for Systems Neuroscience and Centre for the Biology of Memory, Norwegian University of Science and Technology, NO-7489 Trondheim, Norway.

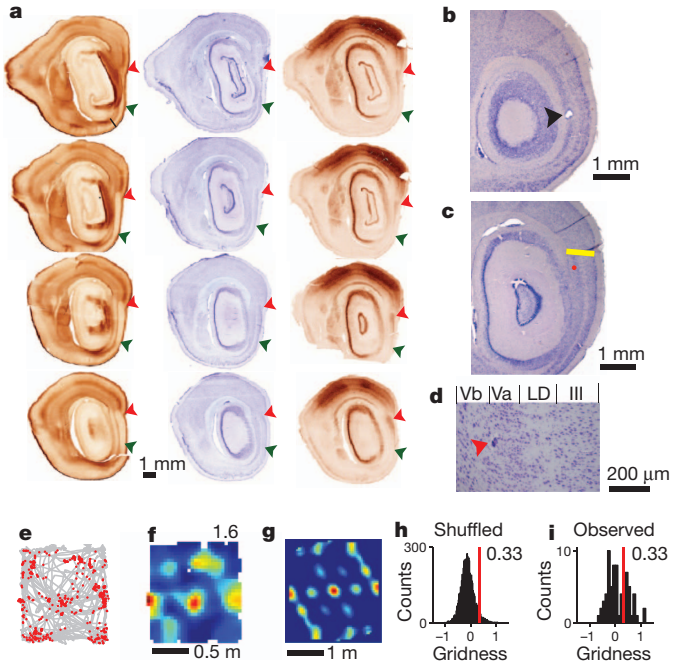

Figure 2 | Anatomical delineation of MEC in Egyptian fruit bats, and targeting of grid cells. **a**, Sagittal sections stained for calretinin (left), Nissl (middle) and parvalbumin (right), arranged from medial (top) to lateral (bottom). Arrowheads indicate MEC borders: dorsal, red; ventral, green. **b**, Electrolytic lesion at the end of a tetrode track (arrowhead). **c**, Recording location in MEC layer V (red dot), close to the dorsal (postrhinal) border of MEC (yellow line). **d**, Higher magnification of the recording location in **c** (arrowhead). MEC layers are indicated on top; LD, *lamina dissecans*[24] (layer IV). **e**–**g**, Grid cell recorded in the MEC location shown in **c**. **e**, Trajectory (grey line) and locations of spikes (red dots), showing the hexagonal firing pattern of a grid cell. **f**, Colour-coded rate map, with peak rate indicated. **g**, Spatial autocorrelogram of the rate map. **h**, Distribution of gridness for shuffled data (Supplementary Information), with 95th percentile indicated (red line; gridness = 0.33). **i**, Histogram of gridness values for all well-separated MEC neurons ($n = 70$). Neurons with gridness >0.33 were defined as grid cells ($n = 25$).

tetrodes were verified histologically by reconstructing the tetrode tracks and by electrolytic lesions (Fig. 2b–d and Supplementary Figs 7–9). Many MEC neurons were active at multiple locations in the arena (for example, Fig. 2e, f), and a hexagonal grid structure was revealed by computing the spatial autocorrelogram of their firing-rate map (Fig. 2g). To quantify the degree of 60° hexagonal rotational symmetry for each neuron, we employed a commonly used 'gridness' index[2] (Supplementary Fig. 10): a higher index indicates a more hexagonal firing field. To test statistically whether a neuron is a grid cell, we used a standard shuffling procedure[4–6] (Fig. 2h, i). Of the 70 well-isolated, behaviourally active neurons recorded in MEC, 36% were classified as grid cells (25 out of 70).

How similar are grid cells in bats versus rats? First, similar to rats[1], grid vertices were separated by 60° angles (Fig. 3a), as expected from a hexagonal structure, and individual firing fields were almost equally spaced (mean standard deviation of grid spacing across the six inner peaks: 6.8 cm; $n = 25$ grid cells). Second, as in rats[1–6], co-localized grid cells in superficial layers of MEC shared similar grid orientation (tilt) and spacing (Fig. 3b and Supplementary Information). Third, as in rats[1], cross-correlating the rate maps of simultaneously recorded grid cells revealed that their maps were offset in phase (Fig. 3c, central peaks of cross-correlograms are offset from the white cross), and the amount of offset spanned all possible phases (Fig. 3d). Fourth, as in rats[1], the grid spacing of individual cells increased with the cell's distance from the postrhinal border (Fig. 3e); this correlation was significant across all neurons ($r = 0.47$, $P < 0.025$), but was even more apparent when analysing separately each bat's data (bat 1, $r = 0.98$, $P < 0.02$; bat 2, $r = 0.67$, $P < 0.05$; bat 3, $r = 0.60$, $P = 0.07$). Fifth, as in rats[2], the firing rate increased with movement velocity (Fig. 3f; t-test, $t_{24} = 2.9$, $P < 0.001$). This correlation of firing rate and velocity probably explains the relatively low firing rates of MEC neurons in crawling bats (Fig. 3e, g) compared to rats[1–3,6], because bats crawled rather slowly (Supplementary Fig. 11). Finally, we found that in bat MEC, the diversity of spatial cell types was very similar to that known from rat MEC[1–6,25] and contained: (1) 'pure grid cells'[1,2] (Fig. 3g, lower-right quadrant; for example, cells 3, 4, 5), with no sensitivity to the animal's head direction[1,2]; (2) 'conjunctive grid cells'[2,6] (Fig. 3g, upper-right quadrant; cell 2), which are grid cells tuned to a specific head direction[2,6]; (3) head-direction cells[2] that have no grid structure (Fig. 3g, upper-left quadrant; cells 8, 9; see also Supplementary Fig. 12); and (4) 'border cells'[25], which fired along geometrical borders of the environment (for example, Fig. 3g, cell 6). Some cells that did not cross the shuffling thresholds still exhibited clear spatial patterns characteristic of grid cells (Fig. 3g, cell 10) or head-direction cells (cell 7). Taken together, these results indicate that the detailed properties of grid cells (and other cell types) in bat MEC were very similar to those in rat MEC.

We next turned to address the central question of this study, and asked whether the grids can exist without key elements of the oscillatory interference models[10–13]—namely, without continuous theta oscillations in the LFP, and in the absence of theta modulation of grid-cell firing. As a first step in studying the LFP in MEC, we examined non-theta-band, high-frequency ripple oscillations, which are most prominent during sleep[20] (Supplementary Fig. 3d). Ripples in bat MEC were very similar in their properties to ripples in rat MEC (Supplementary Fig. 3d–f and Supplementary Text). However, despite the similarity in ripple oscillations, bats differed markedly from rats in the nature of theta oscillations. First, unlike rats[4–6,14,26], we never observed a prominent continuous theta-band oscillation in the LFP, irrespective of the recording site in MEC and the type of reference used (Fig. 4a, b and Supplementary Information). The LFP power-spectrum showed no theta peak, neither during sleep (Supplementary Fig. 13, left), during behaviour (Fig. 4a,b, 'Behav.'), as a function of the animal's velocity (Fig. 4a, b, coloured panels), nor as a function of the bat's echolocation mode[17] (Supplementary Fig. 14a–d). Second, unlike the continuous theta oscillations typically observed in rat MEC[4,5,14,26], theta oscillations in bat MEC occurred in short intermittent bouts, both during behaviour (Fig. 4c–e and Supplementary Fig. 4f, h) and during sleep (Supplementary Fig. 4e, g), similar to bat CA1; 92% of theta bouts during behaviour had duration ≤1 s (Fig. 4d). Theta bouts were separated by very long inter-bout intervals (Fig. 4e; average interval: 37 ± 2 s; 18% of intervals were >1 min). The bat's velocity and echolocation rate were not different during theta bouts versus non-theta epochs (Supplementary Fig. 14e, f). Third, we computed the spike-train temporal autocorrelations for individual grid cells (Fig. 4f, top and Supplementary Fig. 15), and examined the degree of theta modulation in these autocorrelations by computing a standard 'theta index' that was used in previous studies in rats[4–6,26]; this index is based on the relative theta-band power in the Fourier transform of the temporal autocorrelation (Fig. 4g and Supplementary Information). Using either the same criterion that was employed previously to identify theta modulation in rat grid cells[6] (theta index >5), or using a statistical shuffling procedure for each individual spike train, we found that nearly all grid cells in bat MEC (24 out of 25) did not exhibit theta-modulated firing (Fig. 4h, left; theta index across all grid cells 1.29 ± 0.82 (mean ± s.d., maximal value 2.9)), irrespective of the bat's velocity (Supplementary Fig. 16). Because, in the rat MEC, neurons recorded in layers II and III show the most pronounced theta modulation of neuronal firing[6,27], we also analysed separately the data recorded from layers II and III of bat MEC; these analyses showed that no significant theta modulation was present in any of the 35 neurons (of all classes) recorded in layers II and III and in any of the multi-units from these layers (Supplementary Fig. 17). Fourth, because the firing of most neurons in rat MEC (especially in superficial layers) is

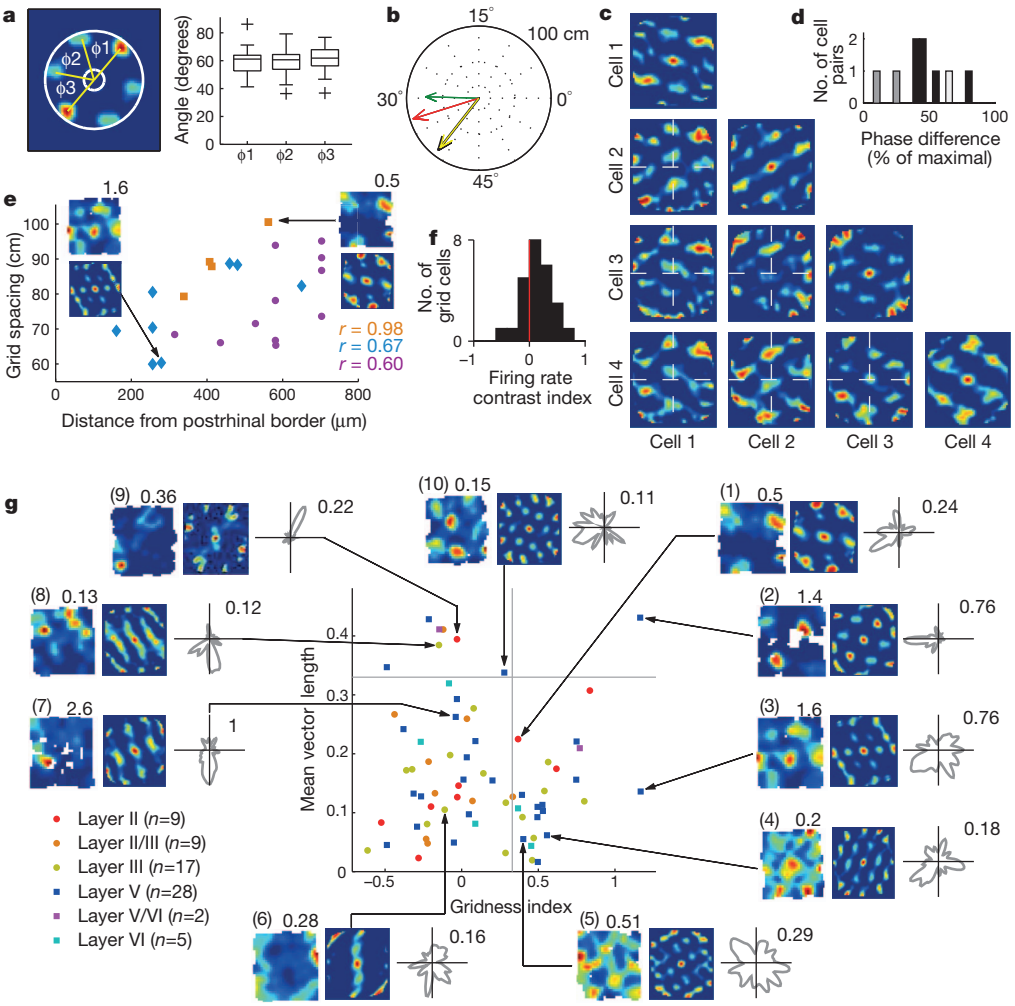

Figure 3 | Grid-cell properties in the bat resemble those in the rat. **a**, Left: definition of the three hexagon angles, depicted on the autocorrelogram annulus of a grid cell. Right: distribution of angles ($n = 25$ grid cells). Box plots show the median angles and interquartile and total ranges; +, outliers. **b**, Polar plot (60° cycle) showing four co-localized grid cells recorded simultaneously on the same tetrode in the superficial layers of MEC, depicting grid spacing (arrow length, cm) and orientation (angle within 60° cycle). Red, green, black and yellow arrows denote these four co-localized grid cells. **c**, Autocorrelograms (diagonal panels) and cross-correlograms (off-diagonal) of the four simultaneously recorded grid cells from **b**. **d**, Distribution of phase differences between pairs of co-localized grid cells. Different shading indicates different recording sites. **e**, Grid spacing increases with distance from postrhinal (dorsal) border of MEC. Colours of dots indicate individual bats and match the colours of *r* values. Insets show firing-rate maps and autocorrelograms of two grid cells recorded at different distances from the postrhinal border. **f**, Distribution of firing-rate contrast indexes for high versus low movement velocity. **g**, Scatter plot of mean vector length index versus gridness index for all neurons from MEC ($n = 70$). Colour and shape of symbols denote recording layer in MEC. Vertical and horizontal lines indicate 95th percentile of shuffled distributions of gridness and mean vector length, respectively. Insets show examples of neurons discussed in the main text, showing (from left to right) the rate map, spatial autocorrelogram and head-direction polar rate plots (grey). Peak firing rate (in Hz) is indicated for rate maps and polar maps.

theta-modulated[6], and they have similar phases[28], we also examined the temporal periodicity of the multi-unit activity, where firing rates are much higher than in individual neurons, and hence oscillations might be detected more robustly. We found that 100% of multi-unit sites where grid cells were recorded (17 out of 17) did not exhibit theta-modulated firing (Fig. 4h, right; theta index 0.97 ± 0.56; maximal value 2.1; see also Supplementary Figs 15–17). Fifth, because rat MEC neurons are often locked to a specific phase of the theta cycle[14,27,28], we examined whether spikes are locked to bats' theta phase during theta bouts. We found that bat MEC neurons indeed exhibited a clear, albeit weak, phase-locking during theta bouts (Fig. 4i, bottom, grey; see also Supplementary Fig. 18). Importantly, no phase locking could be observed outside the theta bouts (Fig. 4i, red). The contrast between phase locking of spikes during theta bouts versus lack of locking outside the bouts (Fig. 4i) indicates that theta bouts in bats are truly discrete and locally generated events. Sixth, to examine the possible contribution of theta bouts to grid formation, we removed in each grid cell all theta-bout epochs, and re-computed the firing-rate maps and two-dimensional autocorrelograms; this did not cause substantial alterations in the grid pattern (Fig. 4j, k and Supplementary Fig. 19). Notably, only a minority of spikes emitted by any single grid cell occurred during theta bouts (4.4 ± 0.75%). In fact, in some grid cells, the grid field existed in the absence of any spikes emitted during theta bouts (Fig. 4k, right; zero spikes emitted during all the theta bouts). Population analysis confirmed that theta-bout removal did not lead to significant changes in gridness values, in any of the grid cells (Fig. 4l, 100% of the cells showed changes in gridness that did not exceed the 95% confidence intervals). This suggests that the grids are maintained during times when theta oscillations are not present.

Taken together, these findings provide the first report on grid cells in a non-rodent species, which supports the generality of the grid-cell phenomenon across mammals; more importantly, our findings causally dissociate the link between the existence of grids and the existence of continuous theta-band oscillations in the mammalian entorhinal

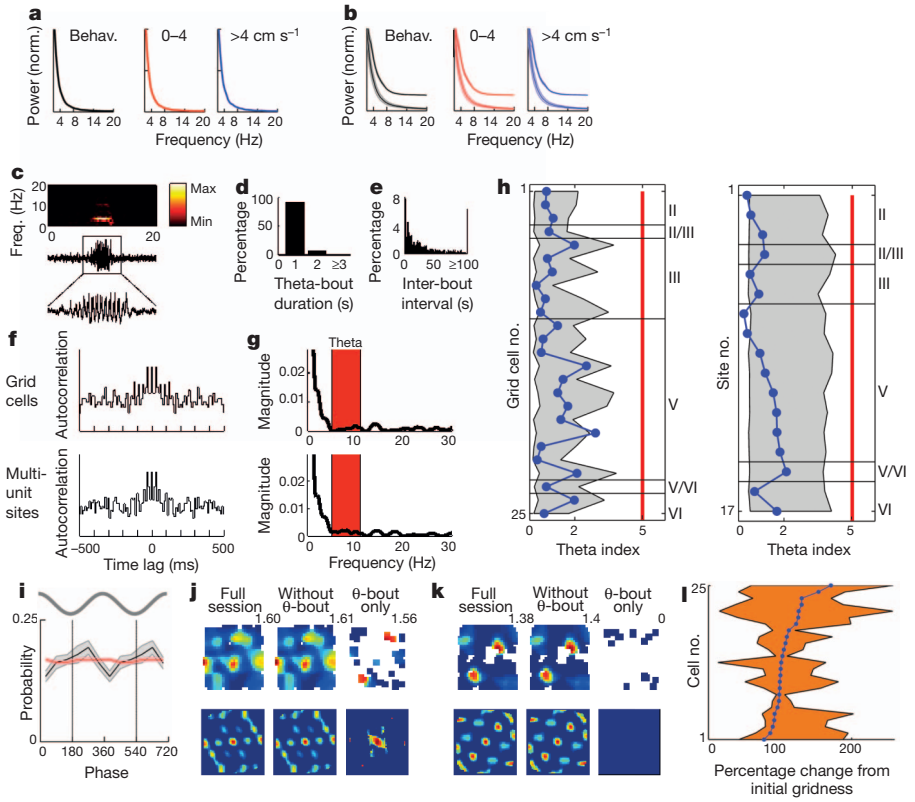

Figure 4 | No continuous theta oscillations in bat MEC. **a**, LFP power spectrum during a single behavioural session (left, Behav.), and separated according to bat's velocity (coloured panels). **b**, Population average LFP power spectrum for all behavioural sessions in which grid cells were recorded (left, Behav.), and separated by velocity (coloured panels). The two lines in each panel show the two reference types used for electrophysiological recordings: single-ended (ground screw, top line) and double-ended (local reference tetrode, bottom); vertical separation is for display purposes only (mean ± s.e.m.). Note the absence of a peak at theta frequency. **c**, LFP trace showing an example theta bout during locomotion. Middle 20-s wideband trace (1–475 Hz). The box around the theta bout serves as calibration bars: 7-s horizontal and 0.4-mV vertical. Bottom: 7-s zoom in. Top: spectrogram. **d**, Distribution of theta-bout durations during behaviour. **e**, Distribution of inter-bout intervals during behaviour. **f**, Spike-train temporal autocorrelograms for a single grid cell (top) and the multi-unit activity recorded at the same site (bottom). Bin size, 10 ms. **g**, Power spectrum of the autocorrelograms in **f**. Note the absence of spectral peak at the theta frequency range (5–11 Hz, highlighted in red). **h**, Theta indexes for grid cells ($n = 25$, left) and multi-unit sites in which grid cells were recorded ($n = 17$, right), arranged by recording layer in MEC (layer number indicated on the right). Shaded area indicates 95% confidence intervals. Notably, 96% (24 out of 25) of grid cells and 100% (17 of 17) of multi-unit sites did not show significant theta modulation, irrespective of the recording layer. **i**, Population average phase histograms of MEC neurons' discharge probability during theta bouts (grey curve) and during non-theta epochs (red). Both curves show mean ± s.e.m. Two theta cycles are shown for visualization purposes. **j**, **k**, Removal of theta bouts: rate maps (top) and spatial autocorrelograms (bottom) of two grid cells (**j** and **k**), for all the data (left), without theta bouts (middle) and during theta bouts only (right). Colour scale of rate maps normalized to maximal firing rate for all three maps for each neuron. **l**, Changes in gridness after theta-bout removal; data for all grid cells (blue dots, sorted) and 95% bootstrap confidence interval (orange area; Supplementary Information) are shown. None of the grid cells showed significant changes in gridness after removal of theta bouts.

cortex. The similarities in the anatomy and grid-cell properties between bats and rats strongly suggest that similar underlying neural mechanisms generate the grid, indicating that the functional dissociation between theta and grids generalizes across mammalian species. Although it is possible that continuous theta oscillations would be found in bats during flight, we emphasize that, under the specific crawling conditions of our experiments, we observed simultaneously the existence of grids without continuous theta oscillations in the LFP or in the spiking activity, which strongly argues against the theta-based class of computational models of grid cells[10–13], but is consistent with the other models which do not rely on theta oscillations[7–9].

Recently, two studies showed that inactivation of medial septum inputs to rat MEC disrupts grid fields, and also disrupts theta oscillations in MEC[28,29]. Additionally, these studies found that, after medial septum inactivation, the firing rates of MEC grid cells dropped by >40%, on average, and in many cases the firing rates dropped threefold and even fivefold[28,29]. These observations have been interpreted as supporting the oscillatory interference models[28,29], but they equally well support network models of grid cells: it is well known in the theory of neural networks that the removal of a major input to a network, if accompanied by a marked decrease in firing rates, can drive the network into a very different activity regime[30], which could disrupt grid formation. Thus, inactivation of a major input to a brain network[28,29] cannot serve to dissociate oscillation-based models from network models. In contrast, our study in bats did not manipulate the inputs to the entorhinal network, and thus provided a unique opportunity to causally challenge the oscillatory interference models of grid cells. More generally, we provide here a rare example of causally disproving a major class of computational models of a higher brain area.

METHODS SUMMARY

Immunohistochemical stainings were conducted to delineate the anatomical location and borders of the medial entorhinal cortex (MEC) in Egyptian fruit bats (*Rousettus aegyptiacus*). Single neuron activity and local field potentials (LFP) were recorded from hippocampal area CA1 and MEC of five bats (two and three bats, respectively), using tetrodes[17–19]. Neuronal activity and positional data were collected while bats foraged in a large arena (117 × 117 cm) in search of food. Place cells[19] in CA1 were identified using a criterion of spatial information >0.5 bits per spike (ref. 17). Grid cells and head-direction cells were identified using a standard gridness index[2] and mean vector length index of the head-direction tuning[4,5]; significance of these two indices was tested using a random shuffling procedure similar to that described previously in rats[4,5]. To quantify grid properties, we computed grid spacing, orientation, phase and velocity-modulation of the cell's

firing[1,2]. High-frequency ripple oscillations in the LFP during sleep were detected as transients in the power of the filtered LFP trace (80–160 Hz) exceeding 7 s.d. above the mean power[17]. Theta oscillation epochs were defined as 2-s windows in which the ratio between the power in the theta (4–8 Hz) and delta (2–4 Hz) frequency ranges exceeded 2.0. Theta modulation of neuronal firing was assessed using a standard theta index, which is based on the spectral power of the spike train temporal autocorrelogram[4–6]. Detailed experimental and analytical procedures are provided in the Supplementary Information.

Received 9 April; accepted 27 September 2011.

1. Hafting, T., Fyhn, M., Molden, S., Moser, M.-B. & Moser, E. I. Microstructure of a spatial map in the entorhinal cortex. *Nature* **436,** 801–806 (2005).
2. Sargolini, F. *et al.* Conjunctive representation of position, direction, and velocity in entorhinal cortex. *Science* **312,** 758–762 (2006).
3. Barry, C., Hayman, R., Burgess, N. & Jeffery, K. J. Experience-dependent rescaling of entorhinal grids. *Nature Neurosci.* **10,** 682–684 (2007).
4. Langston, R. F. *et al.* Development of the spatial representation system in the rat. *Science* **328,** 1576–1580 (2010).
5. Wills, T. J., Cacucci, F., Burgess, N. & O'Keefe, J. Development of the hippocampal cognitive map in preweanling rats. *Science* **328,** 1573–1576 (2010).
6. Boccara, C. N. *et al.* Grid cells in pre- and parasubiculum. *Nature Neurosci.* **13,** 987–994 (2010).
7. Fuhs, M. C. & Touretzky, D. S. A spin glass model of path integration in rat medial entorhinal cortex. *J. Neurosci.* **26,** 4266–4276 (2006).
8. McNaughton, B. L., Battaglia, F. P., Jensen, O., Moser, E. I. & Moser, M.-B. Path integration and the neural basis of the 'cognitive map'. *Nature Rev. Neurosci.* **7,** 663–678 (2006).
9. Burak, Y. & Fiete, I. R. Accurate path integration in continuous attractor network models of grid cells. *PLOS Comput. Biol.* **5,** e1000291 (2009).
10. Burgess, N., Barry, C. & O'Keefe, J. An oscillatory interference model of grid cell firing. *Hippocampus* **17,** 801–812 (2007).
11. Giocomo, L. M., Zilli, E. A., Fransén, E. & Hasselmo, M. E. Temporal frequency of subthreshold oscillations scales with entorhinal grid cell field spacing. *Science* **315,** 1719–1722 (2007).
12. Hasselmo, M. E., Giocomo, L. M. & Zilli, E. A. Grid cell firing may arise from interference of theta frequency membrane potential oscillations in single neurons. *Hippocampus* **17,** 1252–1271 (2007).
13. Blair, H. T., Welday, A. C. & Zhang, K. Scale-invariant memory representations emerge from Moiré interference between grid fields that produce theta oscillations: a computational model. *J. Neurosci.* **27,** 3211–3229 (2007).
14. Hafting, T., Fyhn, M., Bonnevie, T., Moser, M.-B. & Moser, E. I. Hippocampus-independent phase precession in entorhinal grid cells. *Nature* **453,** 1248–1252 (2008).
15. Yovel, Y., Falk, B., Moss, C. F. & Ulanovsky, N. Optimal localization by pointing off axis. *Science* **327,** 701–704 (2010).
16. Ulanovsky, N. & Moss, C. F. What the bat's voice tells the bat's brain. *Proc. Natl Acad. Sci. USA* **105,** 8491–8498 (2008).
17. Ulanovsky, N. & Moss, C. F. Hippocampal cellular and network activity in freely moving echolocating bats. *Nature Neurosci.* **10,** 224–233 (2007).
18. Ulanovsky, N. & Moss, C. F. Dynamics of hippocampal spatial representation in echolocating bats. *Hippocampus* **21,** 150–161 (2011).
19. Wilson, M. A. & McNaughton, B. L. Dynamics of the hippocampal ensemble code for space. *Science* **261,** 1055–1058 (1993).
20. Chrobak, J. J. & Buzsáki, G. High-frequency oscillations in the output networks of the hippocampal-entorhinal axis of the freely behaving rat. *J. Neurosci.* **16,** 3056–3066 (1996).
21. Buzsáki, G. Theta oscillations in the hippocampus. *Neuron* **33,** 325–340 (2002).
22. Stewart, M. & Fox, S. E. Hippocampal theta activity in monkeys. *Brain Res.* **538,** 59–63 (1991).
23. Ekstrom, A. D. *et al.* Human hippocampal theta activity during virtual navigation. *Hippocampus* **15,** 881–889 (2005).
24. Witter, M. P., Wouterlood, F. G., Naber, P. A. & Van Haeften, T. Anatomical organization of the parahippocampal-hippocampal network. *Ann. NY Acad. Sci.* **911,** 1–24 (2000).
25. Solstad, T., Boccara, C. N., Kropff, E., Moser, M.-B. & Moser, E. I. Representation of geometric borders in the entorhinal cortex. *Science* **322,** 1865–1868 (2008).
26. Deshmukh, S. S., Yoganarasimha, D., Voicu, H. & Knierim, J. J. Theta modulation in the medial and the lateral entorhinal cortices. *J. Neurophysiol.* **104,** 994–1006 (2010).
27. Mizuseki, K., Sirota, A., Pastalkova, E. & Buzsáki, G. Theta oscillations provide temporal windows for local circuit computation in the entorhinal-hippocampal loop. *Neuron* **64,** 267–280 (2009).
28. Brandon, M. P. *et al.* Reduction of theta rhythm dissociates grid cell spatial periodicity from directional tuning. *Science* **332,** 595–599 (2011).
29. Koenig, J., Linder, A. N., Leutgeb, J. K. & Leutgeb, S. The spatial periodicity of grid cells is not sustained during reduced theta oscillations. *Science* **332,** 592–595 (2011).
30. Hansel, D. & Sompolinsky, H. Modeling feature selectivity in local cortical circuits. In *Methods in Neuronal Modeling: from Synapses to Networks* 2nd edn (eds Kock, C. & Segev, I.) 499–567 (MIT Press, 1998).

Supplementary Information is linked to the online version of the paper at www.nature.com/nature.

Acknowledgements We thank D. Derdikman, S. Romani, M. Ahrens and Y. Cohen for comments on the manuscript, M. Melcón for initial assistance with hippocampal CA1 recordings, M. Weinberg for veterinary oversight, and R. Eilam and C. Ra'anan for histology. This study was supported by research grants from the Israel Science Foundation and Minerva Foundation to N.U., by a Lev-Zion predoctoral excellence fellowship to M.M.Y., as well as by grants from the Norwegian Research Council and the Kavli Foundation to M.P.W.

Author Contributions M.M.Y. and N.U. designed the study, conducted the experiments, analysed the data and wrote the manuscript. M.P.W. performed immunohistochemical analyses, delineated the anatomical structures in the hippocampus and entorhinal cortex of Egyptian fruit bats, and verified recording sites. All authors discussed the results and commented on the manuscript.

Author Information Reprints and permissions information is available at www.nature.com/reprints. The authors declare no competing financial interests. Readers are welcome to comment on the online version of this article at www.nature.com/nature. Correspondence and requests for materials should be addressed to N.U. (nachum.ulanovsky@weizmann.ac.il).